J Nonlinear Sci (2017) 27:1193–1214
DOI 10.1007/s00332-016-9334-5

Journal of Nonlinear Science

Flight Control of Biomimetic Air Vehicles Using Vibrational Control and Averaging

Sevak Tahmasian[1] · **Craig A. Woolsey**[2]

Received: 26 May 2016 / Accepted: 6 September 2016 / Published online: 19 September 2016

Abstract A combination of vibrational inputs and state feedback is applied to control the flight of a biomimetic air vehicle. First, a control strategy is developed for longitudinal flight, using a quasi-steady aerodynamic model and neglecting wing inertial effects. Vertical and forward motion is controlled by modulating the wings' stroke and feather angles, respectively. Stabilizing control parameter values are determined using the time-averaged dynamic model. Simulations of a system resembling a hawkmoth show that the proposed controller can overcome modeling error associated with the wing inertia and small parameter uncertainties when following a prescribed trajectory. After introducing the approach through an application to longitudinal flight, the control strategy is extended to address flight in three-dimensional space.

Keywords Biomimetic air vehicle · Flapping flight · Averaging · Geometric control

1 Introduction

Bio-inspired engineering involves using examples from nature to solve technical problems (Jenkins 2011). For example, inspired by flying insects, researchers are developing biomimetic air vehicles (BAVs) that can quickly negotiate confined spaces and withstand large disturbances. The engineering design of BAVs involves fluid mechanics, multi-body dynamics, and control theory. Efforts to mimic insect flight have

Communicated by Maurizio Porfiri.

✉ Sevak Tahmasian
sevakt@vt.edu

[1] Department of Biomedical Engineering and Mechanics, Virginia Tech, Blacksburg, VA, USA

[2] Department of Aerospace and Ocean Engineering, Virginia Tech, Blacksburg, VA, USA

improved our knowledge of low Reynolds number, unsteady aerodynamics, nonlinear dynamics and control, and the design and manufacture of microscale mechanisms.

The aerodynamic forces and moments acting on a BAV can be obtained by solving the Navier–Stokes equations with the appropriate boundary conditions, but this approach does not readily support modeling and control design (Ramamurti and Sandberg 2002). Typical studies of insect or BAV dynamics and control adopt a quasi-steady aerodynamic model whose parameters are determined from experimental studies. Most of these quasi-steady models are based on the blade-element method, in which each wing is divided into spanwise sections over which the flow is assumed to be two-dimensional. Integrating the aerodynamic forces and moments along the span yields an estimate of the total aerodynamic contribution of the wing (Ellington 1984). This paper adopts the quasi-steady, blade-element aerodynamic model developed by Deng et al. (2006b).

BAVs are generally underactuated systems resembling flying insects, bats, or birds. Underactuated systems contain fewer actuators than degrees of freedom (DOFs), so a vehicle that flaps appendages for propulsion and control is inherently underactuated. Small-scale BAVs, as opposed to larger ornithopters, use high-frequency flapping to generate sufficient aerodynamic forces to overcome gravity and fly. For example, the nano hummingbird (Keennon et al. 2012) and Harvard microrobotic fly (Wood 2008) use flapping frequencies of 30 and 110 Hz, respectively. Since insects and BAVs use periodic aerodynamic forces generated by flapping their wings, they can be modeled as nonlinear time-periodic (NLTP) systems. The averaging theorem (Guckenheimer and Holmes 1983; Sanders and Verhulst 1985) is often used to construct a nonlinear time-invariant (NLTI) approximation of a high-frequency NLTP system. If the NLTI system has a hyperbolic equilibrium point, then the NLTP system has a corresponding periodic orbit with the same stability properties (Guckenheimer and Holmes 1983).

Early efforts to control a BAV's flight focused on stabilizing hovering flight. For example, Deng et al. (2006a) developed a periodic proportional output feedback control law to stabilize hover. Though the authors mentioned the averaging theorem, they did not determine the averaged dynamics analytically. Instead, they used multiple simulations to determine a linear approximation of the average aerodynamic forces and moments. Khan and Agrawal (2007) discuss the use of differential flatness to develop a nonlinear controller for the longitudinal dynamics of a BAV. In a series of papers, Oppenheimer, Doman, and Sigthorsson describe an approach to three-dimensional motion control of a BAV by modulating the flapping frequency (Oppenheimer et al. 2009; Doman et al. 2010; Oppenheimer et al. 2011). The "split-cycle" waveform modulation technique enables a BAV to generate nonzero time-averaged aerodynamic forces using the waveform parameters as feedback-controlled inputs. Later simulations using high-fidelity dynamic and aerodynamic models demonstrated the robustness of the control method to modeling uncertainties. Another technique, similar to split-cycle control, called "biharmonic amplitude and bias modulation" was developed and tested by Anderson and Cobb (2012, 2014), who also provide a useful summary of the major work on BAVs.

Biological flyers are remarkably robust to disturbances. Several efforts at control design for BAVs have addressed robustness explicitly. Serrani et al. (2010) discusses robust set-point control for the longitudinal motion of a 3-DOF BAV, and Bhatia et al.

(2014) used linear-quadratic regulator theory to address gust resilience. Rifai et al. (2012) discuss the use of bounded state feedback control to robustly regulate a BAV's position and attitude. An empirical approach to maneuver control of an insect-scale BAV is discussed in Ma et al. (2013). Adding adaptive elements to the controller to cope with uncertainties can improve performance (Chirarattananon et al. 2014). Other recent work on longitudinal flight control for insect-scale BAVs is discussed in Elzinga et al. (2014). For recent reviews of dynamic and aerodynamic modeling, stability analysis, and flight control of BAVs, see (Taha et al. 2012; Orlowski and Girard 2012; Sun 2014; Ward et al. 2015).

In this paper, vibrational control and averaging, as discussed in (Bullo 2002; Bullo and Lewis 2005), are used to control the three-dimensional motion of a BAV. Under the proposed high-frequency, high-amplitude control law, the dynamics of the closed-loop mechanical system take the form considered in Bullo (2002). Specifically, the closed-loop dynamics are described by the sum of a slowly varying "drift" vector field and one or more fast-varying input vector fields. Because of the high-frequency, high-amplitude forcing, the drift vector field is a small perturbation, in comparison with the input vector fields. As recognized in Bullo (2002), the structure of the equations suggests the use of the averaging theorem to simplify stability and control analysis. Because the dynamics are averaged over a complete flapping cycle, only one set of averaged equations is needed. The proposed control method is an adaptation of the one developed by Tahmasian et al. (2013); Tahmasian and Woolsey (2015), in which vertical motion is controlled by modulating the stroke amplitude, forward motion is controlled by modulating the feathering angle (the pitch angle of the wing), and lateral motion is controlled by varying these parameters asymmetrically. The pitch attitude is not directly controlled; however, it is passively stable if there is natural pitch damping.

Section 2 discusses vibrational control and averaging of control-affine mechanical control systems. The equations of longitudinal motion of a BAV, including the wing inertia effects, are derived in Sect. 3. By ignoring the wing inertia effects, the equations are transformed to a simpler form that is amenable to the proposed control method. The aerodynamic model is discussed in Sect. 4. In Sect. 5, the proposed control method for control of longitudinal motion is presented, and the performance and robustness of the controller are discussed in the context of numerical simulations. Afterward, the method is extended for control of three-dimensional motion of a BAV, as discussed in Sect. 6. Section 7 reviews the major conclusions from the work and suggests some avenues for continuing research.

2 Vibrational Control and Averaging of Mechanical Control Systems

Consider an n-DOF mechanical control-affine system with m inputs:

$$\ddot{\boldsymbol{q}} = \boldsymbol{f}(\boldsymbol{q}, \dot{\boldsymbol{q}}) + \sum_{i=1}^{m} \boldsymbol{g}_i(\boldsymbol{q}) u_i(t), \qquad \boldsymbol{q}(0) = \boldsymbol{q}_0, \ \dot{\boldsymbol{q}}(0) = \boldsymbol{v}_0 \tag{1}$$

where $\boldsymbol{q} = (q_1, \ \ldots, \ q_n)^T$ is the vector of generalized coordinates, $\boldsymbol{f}(\boldsymbol{q}, \dot{\boldsymbol{q}})$ and $\boldsymbol{g}_i(\boldsymbol{q})$ are smooth vector fields on the state space manifold, and $u_i(t)$ are the inputs.

We impose high-frequency, high-amplitude periodic inputs $u_i(t)$, $i \in \{1, \ldots, m\}$, in the form

$$u_i(t) = \omega v_i(\omega t) \tag{2}$$

where ω is the (high) frequency and $v_i(t)$ is a zero-mean, T-periodic function. Defining the state vector $\boldsymbol{x} = (\boldsymbol{q}^T,\ \dot{\boldsymbol{q}}^T)^T$ and using the inputs defined in (2), system (1) can be written in the first-order form

$$\dot{\boldsymbol{x}} = \boldsymbol{Z}(\boldsymbol{x}) + \sum_{i=1}^{m} \boldsymbol{Y}_i(\boldsymbol{x}) \left(\frac{1}{\epsilon}\right) v_i\left(\frac{t}{\epsilon}\right), \qquad \boldsymbol{x}(0) = \boldsymbol{x}_0 = (\boldsymbol{q}_0^T\ ,\ \boldsymbol{v}_0^T)^T \tag{3}$$

where $\epsilon = 1/\omega$ is a small parameter, $\boldsymbol{Z}(\boldsymbol{x}) = \left(\dot{\boldsymbol{q}}^T,\ \boldsymbol{f}^T(\boldsymbol{q}, \dot{\boldsymbol{q}})\right)^T$ is the drift vector field, and $\boldsymbol{Y}_i(\boldsymbol{x}) = \left(\boldsymbol{0}_{1\times n},\ \boldsymbol{g}_i^T(\boldsymbol{q})\right)^T$ are the input vector fields.

For the zero-mean, periodic inputs (2), we define scalar parameters κ_i, λ_{ij}, and μ_{ij}, for $i, j \in \{1, \ldots, m\}$, as follows: (Tahmasian et al. 2016)

$$\kappa_i = \frac{1}{T} \int_0^T \int_0^t v_i(\tau) d\tau dt \tag{4}$$

$$\lambda_{ij} = \frac{1}{T} \int_0^T \left(\int_0^t v_i(\tau) d\tau\right) \left(\int_0^t v_j(\tau) d\tau\right) dt \tag{5}$$

and

$$\mu_{ij} = \frac{1}{2}(\lambda_{ij} - \kappa_i \kappa_j) \tag{6}$$

Also we define the *symmetric product* between two input vector fields $\boldsymbol{Y}_i(\boldsymbol{x})$ and $\boldsymbol{Y}_j(\boldsymbol{x})$ as

$$\langle \boldsymbol{Y}_i : \boldsymbol{Y}_j \rangle(\boldsymbol{x}) = \langle \boldsymbol{Y}_j : \boldsymbol{Y}_i \rangle(\boldsymbol{x}) = \left[\boldsymbol{Y}_j(\boldsymbol{x}), [\boldsymbol{Z}(\boldsymbol{x}), \boldsymbol{Y}_i(\boldsymbol{x})]\right] \tag{7}$$

where $[\cdot, \cdot]$ denotes the Lie bracket of vector fields.

Theorem 2.1 (Adapted from Bullo and Lewis (2005), Ch. 9) *Consider control-affine system* (1) *with high-frequency, high-amplitude inputs defined as* (2)*, and its first-order form* (3)*. Suppose that* $\boldsymbol{f}(\boldsymbol{q}, \dot{\boldsymbol{q}})$ *and* $\boldsymbol{g}_i(\boldsymbol{q})$ *depend polynomially on their arguments and are twice differentiable in* $\boldsymbol{q}$ *and that the components of* $\boldsymbol{f}(\boldsymbol{q}, \dot{\boldsymbol{q}})$ *are homogeneous in* $\dot{\boldsymbol{q}}$ *of degree two and less. Consider the time-invariant system*

$$\dot{\bar{\boldsymbol{x}}} = \boldsymbol{Z}(\bar{\boldsymbol{x}}) - \sum_{i,j=1}^{m} \mu_{ij} \langle \boldsymbol{Y}_i : \boldsymbol{Y}_j \rangle(\bar{\boldsymbol{x}}) \tag{8}$$

with the initial condition $\bar{\boldsymbol{x}}(0) = \bar{\boldsymbol{x}}_0 = \boldsymbol{x}_0 + \sum_{i=1}^{m} \kappa_i \boldsymbol{Y}_i(\boldsymbol{x}_0)$*, where* $\bar{\boldsymbol{x}} = (\bar{\boldsymbol{q}}^T,\ \dot{\bar{\boldsymbol{q}}}^T)^T$ *is the state vector. There exists a positive* ϵ_0 *(corresponding to a frequency* ω_0*) such that for all* $0 < \epsilon \leq \epsilon_0$ *(equivalently,* $\omega \geq \omega_0$*),* $\boldsymbol{q}(t) = \bar{\boldsymbol{q}}(t) + O(\epsilon)$ *as* $\epsilon \to 0$ *on the time scale 1. Furthermore, if the system* (8) *possesses a hyperbolically stable equilibrium point* $\bar{\boldsymbol{x}}_e$*, then the system* (3) *possesses a hyperbolically stable periodic*

orbit within an $O(\epsilon)$ neighborhood of the equilibrium point $\bar{\boldsymbol{x}}_e$, and the approximation $\boldsymbol{q}(t) = \bar{\boldsymbol{q}}(t) + O(\epsilon)$ is valid for all time $t \geq 0$.

We call the time-invariant system (8) the averaged form of the time-periodic system (3).

The significance of the symmetric product in the averaged dynamics (8) is that it shows the control authority of the system when using inputs (2). Note that for the class of control-affine systems defined in Theorem 2.1, the symmetric product defined in (7) is a $2n \times 1$ vector field with its first n components being zero. The $(n + k)$th, $k \in \{1, \ldots, n\}$, element of the symmetric product $\langle \boldsymbol{Y}_i : \boldsymbol{Y}_j \rangle$, $i, j \in \{1, \ldots, m\}$, shows the effect of the inputs u_i and u_j on coordinate q_k. In this paper, we adopt the model (3) for a BAV, along with its averaged form (8).

3 Equations of Longitudinal Motion

The system considered here comprises a main rigid body and two rigid wings. To describe the motion of the body and the wings, four reference frames are defined as shown in Figs. 1 and 2. First, an inertial frame $\{X, Y, Z\}$ is fixed in space such that the Z-axis points in the local direction of gravity. Second, the body frame $\{x_b, y_b, z_b\}$ is fixed within the main body, with its origin at the body's center of mass. The x_b-axis defines the longitudinal axis of the BAV, the y_b-axis points to starboard, and z_b completes the right-handed orthogonal reference frame. A third frame $\{x, y, z\}$ is pinned to the origin of the inertial frame but rotates with the body, such that the x-, y-, and z-axes remain parallel to the x_b-, y_b-, and z_b-axes, respectively.

A fourth reference frame describes the motion of the wings. In longitudinal flight, the two wings move symmetrically and the y_b-axis remains parallel to the Y-axis. In this case, the motion of both wings can be described using a single reference frame $\{x_w, y_w, z_w\}$, whose origin is fixed at the joint of the right wing with the y_w-axis pointing toward the wing tip. In this paper, the motion of each wing spar is confined to the x_b–y_b plane. This restriction is consistent with observations of biological flyers, for which the wing motion does not deviate from a body-fixed plane. Each wing's motion can be described by two angles: The stroke angle β describes the flapping motion of the wing back and forth and the feather angle η describes the rotation of the wing about the y_w-axis. Since the velocity of the wings is due mainly to the flapping motion, the wing angle of attack is well approximated by the feather angle η (Deng et al. 2006a).

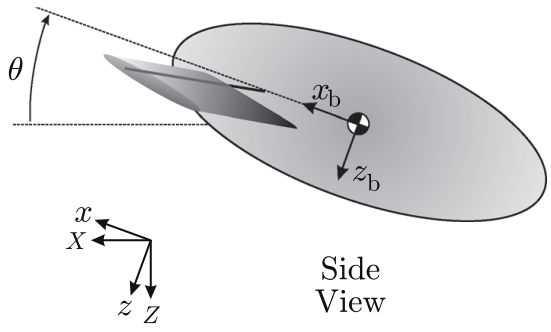

Fig. 1 Inertial and body coordinate frames (side view)

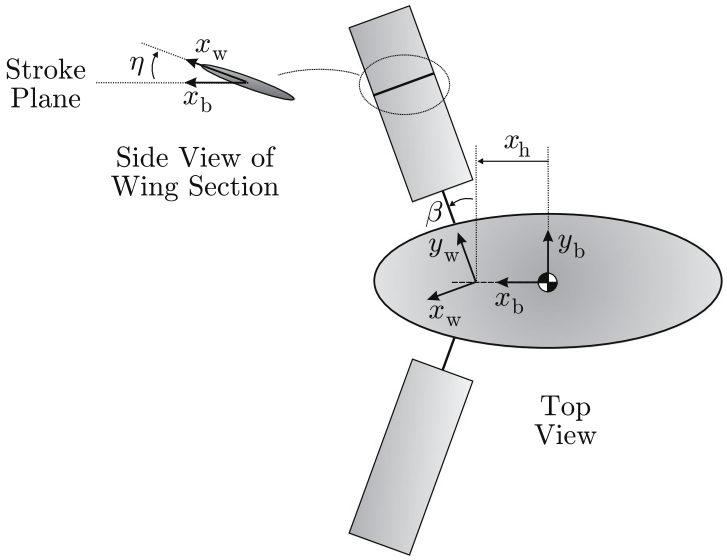

Fig. 2 Wing angles and wing coordinate frame

To derive the equations of motion of the system when considering the wing inertia effects, we use the principle of virtual power (Greenwood 2003). Let $\boldsymbol{i}_\mathrm{b}$, $\boldsymbol{j}_\mathrm{b}$, and $\boldsymbol{k}_\mathrm{b}$ represent the unit vectors defining the body-fixed reference frame. The body translational and rotational velocity in symmetric flight is

$$\boldsymbol{v}_\mathrm{b} = u\boldsymbol{i}_\mathrm{b} + w\boldsymbol{k}_\mathrm{b} \quad \text{and} \quad \boldsymbol{\omega}_\mathrm{b} = \dot{\theta}\,\boldsymbol{j}_\mathrm{b}$$

We define the vector of generalized coordinates for longitudinal flight as $\boldsymbol{q} = (x\,,\,z\,,\,\theta\,,\,\beta)^T$, where x and z are *quasi-coordinates* associated with the body velocity components u and w, respectively, and θ is the body pitch angle.

According to the principle of virtual power

$$\sum_i \left(m_i(\dot{\boldsymbol{v}}_i + \ddot{\boldsymbol{\rho}}_{\mathrm{c}_i}) - \boldsymbol{F}_i\right).\frac{\partial \boldsymbol{v}_i}{\partial \dot{\boldsymbol{q}}_j} + \left(\dot{\boldsymbol{h}}_i + m_i\boldsymbol{\rho}_{\mathrm{c}_i} \times \dot{\boldsymbol{v}}_i - \boldsymbol{M}_i\right).\frac{\partial \boldsymbol{\omega}_i}{\partial \dot{\boldsymbol{q}}_j} = 0 \tag{9}$$

where the index $i \in \{\mathrm{b}, \mathrm{rw}, \mathrm{lw}\}$ represents the three component rigid bodies (body, right wing, and left wing), the index $j \in \{1, 2, 3, 4\}$ refers to the four degrees of freedom represented by the state vector $\boldsymbol{q}$, and m_i, $\boldsymbol{v}_i$, and $\boldsymbol{\omega}_i$ are the mass, velocity of the center of mass, and angular velocity of the ith rigid body, respectively. The vector $\boldsymbol{\rho}_{\mathrm{c}_i}$ points from the reference point of the ith rigid body to its center of mass. (Since the origin of the body frame is set at the body center of mass, $\boldsymbol{\rho}_{c_\mathrm{b}} = \boldsymbol{0}$.) The vector $\boldsymbol{h}_i$ represents the angular momentum of the ith rigid body about the origin of the body frame attached to that rigid body. The vectors $\boldsymbol{F}_i$ and $\boldsymbol{M}_i$ represent the external force and moment acting on the ith rigid body.

For symmetric flight, the body angular momentum is $\boldsymbol{h}_\mathrm{b} = I_y\dot{\theta}\,\boldsymbol{j}_\mathrm{b}$, where I_y is the pitch moment of inertia of the body. Ignoring the aerodynamic effects of the body, the only external force acting on the body is gravity, so $\boldsymbol{F}_\mathrm{b} = -mg\sin\theta\boldsymbol{i}_\mathrm{b} + mg\cos\theta\boldsymbol{z}_\mathrm{b}$ and $\boldsymbol{M}_\mathrm{b} = \boldsymbol{0}$.

Each wing has mass m_w and mass moments of inertia I_{x_w}, I_{y_w}, and I_{z_w} about the x_w-, y_w-, and z_w-axes, respectively. The translational and rotational velocities are

$$\boldsymbol{v}_\mathrm{w} = u\boldsymbol{i}_\mathrm{b} + (w - x_\mathrm{h}\dot{\theta})\boldsymbol{k}_\mathrm{b} \quad \text{and} \quad \boldsymbol{\omega}_\mathrm{w} = \dot{\theta}\,\boldsymbol{j}_\mathrm{b} - \dot{\beta}\boldsymbol{k}_\mathrm{b}$$

where x_h is the longitudinal distance from the origin of the body frame to the origin of the wing frame. The angular velocity vector of the wing can be rewritten in the wing frame as

$$\boldsymbol{\omega}_\mathrm{w}^{(\mathrm{w})} = \begin{pmatrix} \omega_1 \\ \omega_2 \\ \omega_3 \end{pmatrix} = \begin{pmatrix} \dot{\beta}\sin\hat{\eta} - \dot{\theta}\cos\hat{\eta}\sin\beta \\ \dot{\theta}\cos\beta \\ -\dot{\beta}\cos\hat{\eta} - \dot{\theta}\sin\hat{\eta}\sin\beta \end{pmatrix}$$

where we define the convenient shorthand:

$$\hat{\eta}(\eta) = \begin{cases} \eta & ; \quad \dot{\beta} \geq 0 \\ \pi - \eta & ; \quad \dot{\beta} < 0 \end{cases}$$

(Both η and $\hat{\eta}$ are used throughout, depending on which is more convenient.)

The position vector pointing from the hinge root to the wing center of mass is $\boldsymbol{\rho}_{\mathrm{c}_\mathrm{w}} = -x_\mathrm{c}\boldsymbol{i}_\mathrm{w} + y_\mathrm{c}\boldsymbol{j}_\mathrm{w}$. One may compute

$$\ddot{\boldsymbol{\rho}}_{\mathrm{c}_\mathrm{w}}^{(\mathrm{w})} = \begin{pmatrix} \ddot{\rho}_1 \\ \ddot{\rho}_2 \\ \ddot{\rho}_3 \end{pmatrix} = \begin{pmatrix} x_\mathrm{c}(\omega_2^2 + \omega_3^2) - y_\mathrm{c}(\dot{\omega}_3 - \omega_1\omega_2) \\ -x_\mathrm{c}(\dot{\omega}_3 + \omega_1\omega_2) - y_\mathrm{c}(\omega_1^2 + \omega_3^2) \\ x_\mathrm{c}(\dot{\omega}_2 - \omega_1\omega_3) + y_\mathrm{c}(\dot{\omega}_1 + \omega_2\omega_3) \end{pmatrix}$$

The time derivative of the wing angular momentum can be expressed in the wing frame as

$$\dot{\boldsymbol{h}}_\mathrm{w}^{(\mathrm{w})} = \begin{pmatrix} \dot{h}_1 \\ \dot{h}_2 \\ \dot{h}_3 \end{pmatrix} = \begin{pmatrix} I_{x_\mathrm{w}}\dot{\omega}_1 + (I_{z_\mathrm{w}} - I_{y_\mathrm{w}})\omega_2\omega_3 \\ I_{y_\mathrm{w}}\dot{\omega}_2 + (I_{x_\mathrm{w}} - I_{z_\mathrm{w}})\omega_1\omega_3 \\ I_{z_\mathrm{w}}\dot{\omega}_3 + (I_{y_\mathrm{w}} - I_{x_\mathrm{w}})\omega_1\omega_2 \end{pmatrix}$$

The external forces acting on the wings are the gravitational and aerodynamic forces. Since the lateral aerodynamic forces of the two wings are equal and opposite, they cancel. Therefore, the vector of the external forces $\boldsymbol{F}_\mathrm{w}$ expressed in the body frame is

$$\boldsymbol{F}_\mathrm{w}^{(\mathrm{b})} = \begin{pmatrix} F_x - m_\mathrm{w} g\sin\theta \\ 0 \\ F_z + m_\mathrm{w} g\cos\theta \end{pmatrix}$$

where F_x and F_z are the aerodynamic forces acting in x_b and z_b directions, respectively.

The moments applied on the system include the moment due to the weight of the wings, the aerodynamic moment, and the control moment acting on the wings. The moment due to gravity is $\boldsymbol{M}_{g_\mathrm{w}} = (-d\boldsymbol{i}_\mathrm{w} + r_{cg}\boldsymbol{j}_\mathrm{w}) \times m_\mathrm{w} g\boldsymbol{k}_\mathrm{i}$ (where $\boldsymbol{k}_\mathrm{i}$ is the unit vector in the direction of gravity) and the control moment is $\boldsymbol{M}_\mathrm{c} = M_\beta\boldsymbol{k}_\mathrm{b}$. We also consider

a small damping moment acting against the pitch motion of the vehicle with damping coefficient c_{q} attributed to the main body of the vehicle. Substituting these terms in Eq. (9) and simplifying, the longitudinal equations of motion are

$$\begin{cases} F_x = & m(\dot{u} + w\dot{\theta} + g\sin\theta) + m_{\mathrm{w}}(\ddot{\rho}_1\cos\hat{\eta}\cos\beta + \ddot{\rho}_2\sin\beta + \ddot{\rho}_3\sin\hat{\eta}\cos\beta - x_{\mathrm{h}}\dot{\theta}^2) \\ F_z = & m(\dot{w} - u\dot{\theta} - g\sin\theta) + m_{\mathrm{w}}(\ddot{\rho}_3\cos\hat{\eta} - \ddot{\rho}_1\sin\hat{\eta} - x_{\mathrm{h}}\ddot{\theta}) \\ M_y = & m_{\mathrm{w}}\big(d\dot{u}\sin\hat{\eta} + (d\cos\hat{\eta}\cos\beta - r_{\mathrm{cg}}\sin\beta - x_{\mathrm{h}})\dot{w} + x_{\mathrm{h}}\ddot{\theta}(x_{\mathrm{h}} - d\cos\hat{\eta}\cos\beta + r_{\mathrm{cg}}\sin\beta) \\ & + x_{\mathrm{h}}(\ddot{\rho}_1\sin\hat{\eta} - \ddot{\rho}_3\cos\hat{\eta} + u\dot{\theta} + g\cos\theta) - (d\cos\hat{\eta}\cos\beta - r_{\mathrm{cg}}\sin\beta)(u\dot{\theta} + g) \\ & + d\dot{\theta}(w - x_{\mathrm{h}}\dot{\theta})\sin\hat{\eta}\big) + I_y\ddot{\theta} + \dot{h}_2\cos\beta - \dot{h}_1\cos\hat{\eta}\sin\beta - \dot{h}_3\sin\hat{\eta}\sin\beta - c_{\mathrm{q}}\dot{\theta} \\ M_\beta = & m_{\mathrm{w}}(d\cos\hat{\eta}\sin\beta + r_{\mathrm{cg}}\cos\beta)(\dot{u} + (w - x_{\mathrm{h}}\dot{\theta})\dot{\theta}) + \dot{h}_1\sin\hat{\eta} - \dot{h}_3\cos\hat{\eta} \end{cases} \tag{10}$$

where M_y is the aerodynamic moment about the y_{b}-axis and M_β is the stroke control moment applied to the right wing. (In symmetric flight, the left wing moves in unison with the right.)

The inertial effects of the wings on the main body are of small magnitude and may be omitted for control design (Sun et al. 2007; Taha et al. 2012). Therefore, rather than use Eq. (10), we use simpler equations that omit the mutual inertial effects of the wings and body on one another, such that the motion of the main body can be represented using a conventional fixed-wing aircraft model (Etkin 1972). In this case, the equations of motion take the form

$$\begin{cases} \dot{u} &= -qw - g\sin\theta + \frac{1}{m}F_x \\ \dot{w} &= qu + g\cos\theta + \frac{1}{m}F_z \\ \dot{q} &= \frac{1}{I_y}(M_y - c_{\mathrm{q}}q) \\ \ddot{\beta} &= \frac{1}{I^{\mathrm{w}}_{z_{\mathrm{b}}}}M_\beta \end{cases} \tag{11}$$

where $q = \dot{\theta}$ is the pitch rate of the body and $I^{\mathrm{w}}_{z_{\mathrm{b}}} = I_{x_{\mathrm{w}}}\sin^2\hat{\eta} + I_{z_{\mathrm{w}}}\cos^2\hat{\eta}$ is the mass moment of inertia of the right wing about the z_{b}-axis.

Letting U and W denote the inertial components of forward and downward velocity, respectively, the translational kinematic equations are

$$\begin{pmatrix} \dot{X} \\ \dot{Z} \end{pmatrix} = \begin{pmatrix} U \\ W \end{pmatrix} = \begin{pmatrix} \cos\theta & \sin\theta \\ -\sin\theta & \cos\theta \end{pmatrix}\begin{pmatrix} u \\ w \end{pmatrix}$$

Rewriting Eq. (11) in the inertial frame gives

$$\begin{cases} \dot{U} &= \frac{1}{m}F_X \\ \dot{W} &= g + \frac{1}{m}F_Z \\ \dot{q} &= \frac{1}{I_y}(M_y - c_{\mathrm{q}}q) \\ \ddot{\beta} &= \frac{1}{I^{\mathrm{w}}_{z_{\mathrm{b}}}}M_\beta \end{cases} \tag{12}$$

where

$$\begin{pmatrix} F_X \\ F_Z \end{pmatrix} = \begin{pmatrix} \cos\theta & \sin\theta \\ -\sin\theta & \cos\theta \end{pmatrix}\begin{pmatrix} F_x \\ F_z \end{pmatrix}$$

4 Aerodynamic Model

The aerodynamic force and moment are determined using a quasi-steady blade-element model (Deng et al. 2006a, b). The model includes both the translational and rotational effects of the wing motion. Here, we consider a single wing among a pair that moves symmetrically, recognizing that the total contribution will be doubled. We later relax the assumption of symmetric flapping.

The feather (wing pitch) kinematics are prescribed in the following form: $\eta(t) = \eta_0 \,\mathrm{sgn}(\dot{\beta})$, where sgn represents the signum function (Deng et al. 2006a, b). Thus, the feather angle remains at a constant value η_0 during the forward stroke and reverses sign when the stroke motion reverses. The normal and tangential aerodynamic forces are

$$\begin{aligned} F_N &= \frac{1}{2}\rho A_{\mathrm{w}} C_N v_{\mathrm{cp}}^2 \\ F_T &= \frac{1}{2}\rho A_{\mathrm{w}} C_T v_{\mathrm{cp}}^2 \end{aligned} \tag{13}$$

where v_{cp} is the velocity of the center of pressure of the wing, ρ is the density of the fluid, A_{w} is the surface area of the wing, and C_N and C_T are force coefficients. Since the wings undergo high-frequency flapping motion, assuming the body is moving slowly compared with the wings' velocities, almost all of the translational velocity of a blade element of the wing at a distance r from the joint (root) of the wing is due to the flapping motion. (In simulations, the induced angle of attack due to the body motion is retained.) So the velocity of the center of pressure of the wing can be considered as $v_{\mathrm{cp}} \approx r_{\mathrm{cp}}\dot{\beta}$, where r_{cp} denotes the position of the center of pressure in the y_{w} direction (Deng et al. 2006b):

$$r_{\mathrm{cp}} = \sqrt{\frac{\int_0^R c(r) r^2 dr}{A_{\mathrm{w}}}} \tag{14}$$

where R is the wing semi-span and $c(r)$ is the chord length at a distance r from the wing joint in the y_{w} direction. Substituting v_{cp} into (13) gives

$$\begin{aligned} F_N &= \frac{1}{2}\rho A_{\mathrm{w}} C_N r_{\mathrm{cp}}^2 \dot{\beta}^2 \\ F_T &= \frac{1}{2}\rho A_{\mathrm{w}} C_T r_{\mathrm{cp}}^2 \dot{\beta}^2 \end{aligned} \tag{15}$$

Based on experiments, the normal and tangential force coefficients C_N and C_T take the form (Deng et al. 2006b)

$$\begin{aligned} C_N &= \bar{C}_N \,\mathrm{sgn}(\dot{\beta}) \sin\eta \\ C_T &= \bar{C}_T \,\mathrm{sgn}(\dot{\beta}) \cos^2 2\eta \end{aligned} \tag{16}$$

where $\bar{C}_N$ and $\bar{C}_T$ are constant parameters.

There is another component of the normal force due to feathering (pitching) of the wings:

$$F_{r,N} = \frac{1}{2}\rho A_{\mathrm{w}} \bar{C}_r c_{\max} \dot{\eta} v_{\mathrm{cp}}$$

where $\bar{C}_r$ is a force coefficient and $c_{\max}$ is the maximum chord of the wing. Since the feather angle η is assumed to remain constant during each half stroke of the wings, however, this normal force vanishes. (During stroke transitions, when the feather angle changes sign, the stroke velocity $\dot{\beta}$ goes to zero so that $v_{\mathrm{cp}} \approx 0$.)

To use the aerodynamic forces in the equations of motion, the components of the normal and tangential forces in the body frame can be expressed as

$$\begin{pmatrix} F_x \\ F_z \end{pmatrix} = \begin{pmatrix} \cos\theta & \sin\theta \\ -\sin\theta & \cos\theta \end{pmatrix} \begin{pmatrix} F_X \\ F_Z \end{pmatrix} = \begin{pmatrix} \cos\theta & \sin\theta \\ -\sin\theta & \cos\theta \end{pmatrix} \begin{pmatrix} \cos\beta & 0 \\ 0 & 1 \end{pmatrix} \begin{pmatrix} \cos\eta & \sin\eta \\ -\sin\eta & \cos\eta \end{pmatrix} \begin{pmatrix} F_T \\ F_N \end{pmatrix} \tag{17}$$

The aerodynamic moment M_y is the moment of the normal and tangential forces about the center of mass of the body:

$$M_y = r_{\mathrm{cp}}(F_T \sin\eta - F_N \cos\eta)\sin\beta - \frac{1}{4}\bar{c} F_N \mathrm{sgn}(\dot{\beta})\cos\beta \tag{18}$$

where $\bar{c}$ is the mean geometric chord of the wing.

Using Eqs. (15) through (18) and after some calculations, the components of aerodynamic force and moment in the inertial frame can be written as

$$\begin{aligned} F_X &= f_X(\theta, \eta, \beta)\dot{\beta}^2 \\ F_Z &= f_Z(\theta, \eta, \beta)\dot{\beta}^2 \\ M_y &= m_y(\theta, \eta, \beta)\dot{\beta}^2 \end{aligned} \tag{19}$$

where

$$\begin{aligned} f_X =& \frac{1}{2}\rho A_{\mathrm{w}} r_{\mathrm{cp}}^2 \big((\bar{C}_N \cos\eta - \bar{C}_T \cos^2 2\eta)\sin\eta \sin\theta \\ &+ (\bar{C}_N \sin^2\eta + \bar{C}_T \cos\eta \cos^2 2\eta)\cos\beta\cos\theta\big)\mathrm{sgn}(\dot{\beta}) \\ f_Z =& \frac{1}{2}\rho A_{\mathrm{w}} r_{\mathrm{cp}}^2 \big((\bar{C}_N \cos\eta - \bar{C}_T \cos^2 2\eta)\sin\eta\cos\theta - (\bar{C}_N \sin^2\eta \\ &+ \bar{C}_T \cos\eta\cos^2 2\eta)\cos\beta\sin\theta\big)\mathrm{sgn}(\dot{\beta}) \\ m_y =& \frac{1}{2}\rho A_{\mathrm{w}} r_{\mathrm{cp}}^2 \big(r_{\mathrm{cp}}(\bar{C}_T \cos^2 2\eta \\ &- \bar{C}_N \cos\eta)\mathrm{sgn}(\dot{\beta})\sin\beta - \frac{1}{2}\bar{c}\bar{C}_N \cos\beta\big)\sin\eta \end{aligned}$$

The aerodynamic force and moment components required to determine the motion of the system are expressed as functions of the body pitch angle θ, and the wing stroke and feather angles β and η. Recall that, because the analysis above concerned a single

wing, the force and moment components f_X, f_Z, and m_y in (19) are doubled for two wings in symmetric motion.

5 Averaging and Control of Longitudinal Flight

Substituting the force and moment components F_X and F_Y and the moment M_y from (19) into (12), including the contributions from both wings, the dynamic equations of the system can be written succinctly as follows:

$$\begin{aligned}
\dot{U} &= \frac{1}{m} f_X(\theta, \eta, \beta)\dot{\beta}^2 \\
\dot{W} &= g + \frac{1}{m} f_Z(\theta, \eta, \beta)\dot{\beta}^2 \\
\dot{q} &= \frac{1}{I_y}\left(m_y(\eta, \beta)\dot{\beta}^2 - c_{\mathrm{q}} q\right) \\
\ddot{\beta} &= \frac{1}{I^{\mathrm{w}}_{z_{\mathrm{b}}}} M_\beta
\end{aligned} \tag{20}$$

where the stroke control moment M_β and the feather angle η are the control inputs of the system. The goal is to determine the inputs such that the system follows a *slowly varying* desired trajectory $(X_{\mathrm{d}}(t), Z_{\mathrm{d}}(t), \theta_{\mathrm{d}}(t))$ on average.

5.1 Vibrational Control and Averaging for the BAV in Longitudinal Flight

In this paper, we use the feather angle η to control the horizontal motion of the vehicle, and adjust the amplitude of the stroke angle of the wings to control the vertical motion (Dickinson et al. 1999). If the feather angle η and the wing stroke angle β follow zero-mean, periodic profiles, then the net horizontal force generated during one flapping cycle will be zero. If the feather angle differs slightly when the wing is sweeping forward than when it sweeps back, however, there will be a nonzero net horizontal force which can be used to control the horizontal motion of the vehicle. To control the horizontal motion, a proportional-derivative (PD) controller is used to adjust the amplitude of the feather angle of the wing. Specifically, we define

$$\eta = \eta_s + \eta_x$$

where

$$\eta_s = \eta_0 \mathrm{sgn}(\dot{\beta})$$

represents the nominal feather angle required for balanced flight and

$$\eta_x = k_{\mathrm{p}_x}(X_{\mathrm{d}}(t) - X) + k_{\mathrm{d}_x}(\dot{X}_{\mathrm{d}}(t) - \dot{X})$$

is a feedback correction based on the longitudinal position error, with PD control parameters k_{p_x} and k_{d_x}. Provided η_x is small relative to η_s, one can make the following approximations:

$$\begin{aligned} \sin\eta &= \sin(\eta_s) + \eta_x \cos(\eta_s) \\ \cos\eta &= \cos(\eta_s) - \eta_x \sin(\eta_s) \end{aligned} \tag{21}$$

Altitude control can be achieved by adjusting the amplitude of the stroke angle. Using Eq. (12), the simplified dynamic equation for the stroke motion of each wing is

$$\ddot{\beta} = \frac{1}{I^{\mathrm{w}}_{z\mathrm{b}}} M_\beta \tag{22}$$

To modulate the stroke amplitude, we choose (Tahmasian and Woolsey 2015)

$$M_\beta = k_{p_\beta}\beta + k_{d_\beta}\dot{\beta} + B_0(t)\left(1 + k_{p_z}\left(Z_{\mathrm{d}}(t) - Z\right)\right)\omega\cos\omega t \tag{23}$$

where $B_0(t)$ is a time-varying parameter and k_{p_β}, k_{d_β}, and k_{p_z} are control parameters to be determined. By choosing the control moment M_β as (23), the stroke amplitude is adjusted using the altitude tracking error $Z_{\mathrm{d}}(t) - Z$. Defining the state vector $\boldsymbol{x} = \left(X, Z, \theta, \beta, U, W, q, \omega_\beta\right)^T$, with $\omega_\beta = \dot{\beta}$, and using Eqs. (21) through (23), the equations of motion of the system can be written as

$$\dot{\boldsymbol{x}} = \boldsymbol{f}(\boldsymbol{x}, t) + \boldsymbol{g}(\boldsymbol{x}, t)\omega\cos\omega t \tag{24}$$

where

$$\boldsymbol{f}(\boldsymbol{x}, t) = \begin{pmatrix} \dot{X} \\ \dot{Z} \\ q \\ \omega_\beta \\ \frac{1}{m} f_X \omega_\beta^2 \\ g + \frac{1}{m} f_Z \omega_\beta^2 \\ \frac{1}{I_y}\left(m_y \omega_\beta^2 - c_{\mathrm{q}} q\right) \\ \frac{1}{I^{\mathrm{w}}_{z\mathrm{b}}}\left(k_{p_\beta}\beta + k_{d_\beta}\omega_\beta\right) \end{pmatrix}$$

and

$$\boldsymbol{g}(\boldsymbol{x}, t) = \begin{pmatrix} \mathbf{0}_{7\times 1} \\ \frac{B_0(t)}{I^{\mathrm{w}}_{z\mathrm{b}}}\left(1 + k_{p_z}(Z_{\mathrm{d}}(t) - Z)\right) \end{pmatrix}$$

Equation (24) is in the form discussed in Sect. 2. Using Theorem 2.1, the averaged dynamics of the system (24) can be written as

$$\dot{\bar{\boldsymbol{x}}} = \boldsymbol{f}(\bar{\boldsymbol{x}}, t) - \frac{1}{4}\langle \boldsymbol{g} : \boldsymbol{g} \rangle(\bar{\boldsymbol{x}}, t) \tag{25}$$

The symmetric product in (25) is easily computed using symbolic mathematics software, but the resulting expressions are too lengthy to be shown here.

From the structure of the input vector field $\boldsymbol{g}$, one may infer that the input does not directly affect vertical motion. The component of the input vector field $\boldsymbol{g}$ corresponding to vertical acceleration is zero. However, the component of the symmetric product $\langle \boldsymbol{g} : \boldsymbol{g} \rangle$ corresponding to vertical acceleration is nonzero, so a periodic input introduces a vertical force in (25) parameterized by $B_0(t)$. Thus, vertical motion may be controlled using the input M_β.

For a system to track a desired trajectory, that trajectory should be dynamically feasible; i.e., it should satisfy the equations of motion. For the BAV system to follow some desired, slowly varying time histories $X_\mathrm{d}(t)$, $Z_\mathrm{d}(t)$, and $\theta_\mathrm{d}(t)$ on average, these time histories must be consistent with the averaged dynamic equations. To find the parameter $B_0(t)$, we substitute the desired time histories into the vertical dynamic equation of the averaged dynamics and seek a time-varying parameter value $B_0(t)$ for which the equation holds identically. To keep the body pitch angle small, we choose $\theta_\mathrm{d}(t) = 0$. Also note that, because the wings perform high-frequency, zero-mean periodic motion, $\bar{\beta} \equiv 0$. From the sixth component equation of (25), we find that

$$B_0(t) = \frac{I^\mathrm{w}_{z_\mathrm{b}}}{r_\mathrm{cp}} \sqrt{\frac{4m\big(g - \ddot{Z}_\mathrm{d}(t)\big)}{2\rho A_\mathrm{w}\big(\bar{C}_T(1 + \cos 4\eta_0) - 2\bar{C}_N \cos\eta_0\big)\sin\eta_0}} \tag{26}$$

Having determined $B_0(t)$, one may substitute it into the averaged equations of motion (25) and seek parameters k_{p_β}, k_{d_β}, k_{p_z}, k_{p_x}, and k_{d_x} to meet stability and performance requirements. To simplify stability analysis, the nonlinear averaged dynamics (25) can be linearized about the slowly varying desired trajectory to obtain a linear, time-varying perturbation system. In cases where the desired trajectory (for the average motion) is constant, the system obtained from linearization will be linear, time invariant, which considerably simplifies the analysis.

5.2 Simulation and Numerical Results

In this section, the proposed flight control method is applied to a BAV with physical parameters resembling those of a hawkmoth. For simplicity, however, the wings are modeled as (rigid) rectangles with chord length $c = 18.5$ mm and semi-span $R = 52$ mm. The remaining physical parameters follow, some defined by Berman and Jane (2007); Deng et al. (2006b):

$$m = 1.6 \times 10^{-3}\,\mathrm{kg}, \quad I_y = 10^{-6}\,\mathrm{kg\,m^2}, \quad I^\mathrm{w}_{z_\mathrm{b}} = 2 \times 10^{-8}\,\mathrm{kg\,m^2}, \quad \rho = 1.2\,\mathrm{kg\,m^{-3}}$$
$$\eta_0 = 40^\circ, \quad x_\mathrm{h} = 0, \quad \omega = 56\pi\,\mathrm{rad\,s^{-1}}, \quad \bar{C}_N = -3.4, \quad \bar{C}_T = -0.4, \quad c_\mathrm{q} = 10^{-5}\,\mathrm{N\,m\,s}$$

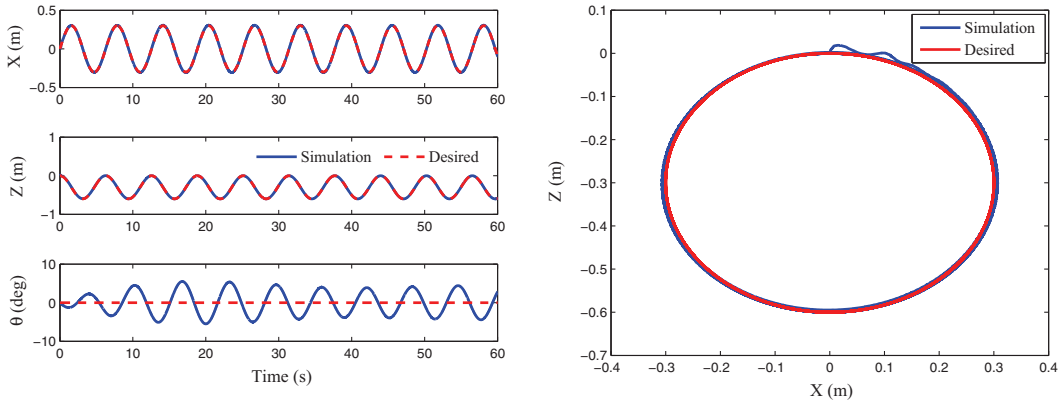

Fig. 3 Simulation results for a circular desired path, neglecting wing inertial effects. **a** Time histories of X, Z, and θ, **b** X–Z path

The control moment M_β defined in (23) makes the averaged vertical motion stable, but not asymptotically stable. To generate a vertical asymptotically stable motion on average, we amend the control moment by adding derivative feedback in Z as follows

$$M_\beta(t) = k_{p_\beta}\beta + k_{d_\beta}\omega_\beta + B_0(t)\left(1 + k_{p_z}\left(Z_\mathrm{d}(t) - Z\right) + k_{d_z}\left(\dot{Z}_\mathrm{d}(t) - \dot{Z}\right)\right)\omega\cos\omega t$$

Omitting units, we choose the control parameters as

$$k_{\mathrm{p}x} = -10, \quad k_{\mathrm{d}x} = -0.6, \quad k_{p_\beta} = -8\times10^{-5}, \quad k_{d_\beta} = -2\times10^{-7}, \quad k_{p_z} = -80, \quad k_{d_z} = -1.2$$

In developing the control method, we assumed that the wing angle of attack is well approximated by η_0. In the simulations, however, the effect of the body's translational motion on the wing angle of attack has been incorporated:

$$\eta = \eta_s + \alpha_\mathrm{b} + \eta_x \tag{27}$$

where α_b represents the angle of attack contribution due to the body's motion:

$$\alpha_\mathrm{b} = \tan^{-1}\frac{w - r_\mathrm{cp}\dot{\beta}\sin\beta}{V}\mathrm{sgn}(\dot{\beta}) \qquad \text{where} \qquad V = \sqrt{(r_\mathrm{cp}\dot{\beta} + u\cos\beta)^2 + w^2} \tag{28}$$

The BAV was tasked with tracking a circular path in vertical X–Z plane with $X_\mathrm{d}(t) = 0.3\sin(t)$ m and $Z_\mathrm{d}(t) = -0.3 + 0.3\cos(t)$ m. The simulation results are presented in Fig. 3a, b. After small deviations at the beginning of motion, the vehicle starts to follow. (Recall that Z is positive downward.)

As evidence of the controller's robustness, the simulations were also performed with the inertial effect of the wings incorporated into the model. The physical properties of the wings are

$$m_\mathrm{w} = 2\times10^{-4}\ \mathrm{kg}, \quad I_{x_\mathrm{w}} = I_{y_\mathrm{w}} = I_{z_\mathrm{w}} = 10^{-6}\ \mathrm{kg\,m^2}$$

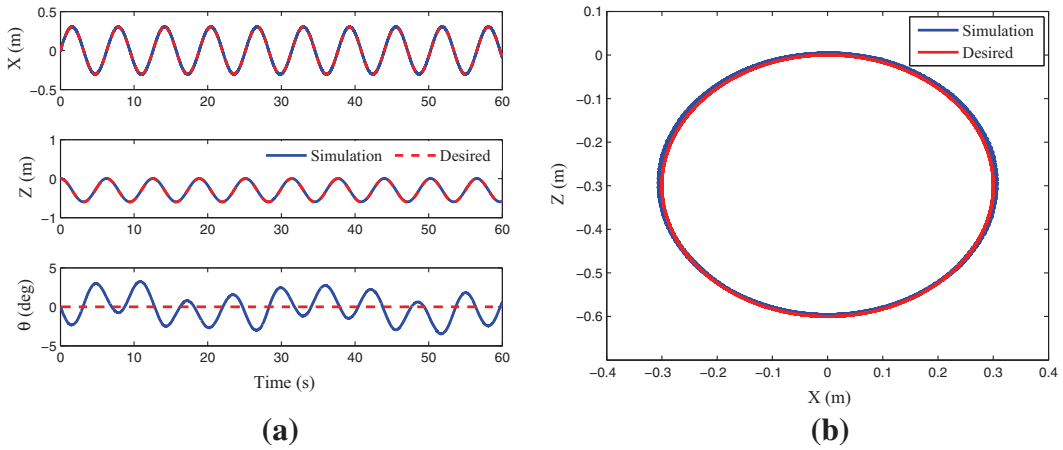

Fig. 4 Simulation results for a circular desired path, including wing inertial effects. **a** Time histories of X, Z, and θ, **b** X–Z path

with the center of mass of each wing at its geometric center. The mass and the mass moments of inertia given here were intentionally chosen larger than the values for a hawkmoth, as a further indication of controller robustness. Applying the controller developed for the simpler model, and using Eq. (10), it is evident in Fig. 4a, b that the controller performs properly even with this multi-body perturbation in the dynamic model.

6 Control of Three-Dimensional Flight

In this section, the controller developed earlier is extended to the problem of three-dimensional (3-D) trajectory tracking. In this case, the main body moves in all six degrees of freedom. Rotational motions are parametrized by the roll (ϕ), pitch (θ), and yaw (ψ) angles. For motion in the body longitudinal plane, the method discussed in Sect. 5 is used. To control roll and yaw attitude and lateral translation, we introduce asymmetry into the wing motion. Thus, we define angles $\beta_{\mathrm{rw}}(t)$ and $\beta_{\mathrm{lw}}(t)$ for the stroke angles of the right and left wings, respectively. The two waveforms will have the same frequency but, in general, different amplitudes. Also, the two wings may use different feather angles η_{rw} and η_{lw}. Asymmetric feather angles are used to control the yaw angle (ψ), and thus the inertial direction of forward flight. Since flapping with different wing feather angles also produces a nonzero lateral force, the vehicle deviates from the desired trajectory when undergoing a yaw motion. Lateral motion is controlled by modulating the vehicle's roll angle (ϕ) with differential stroke angle amplitudes.

6.1 Equations of Three-Dimensional Motion

To simplify control design and analysis, wing inertial effects are neglected when considering the 3-D dynamics. Recall that the multi-body effect of the wings had little impact on the closed-loop performance in the simulations described in the previous

section. Let $\boldsymbol{X} = (X, Y, Z)^T$ represent the position of the body frame in the inertial frame and let $\boldsymbol{x} = (x, y, z)^T$ represent the same position vector in a rotating frame pinned at the origin of the inertial frame. The transformation matrix $\boldsymbol{R}$ from the inertial frame to the rotating frame is

$$\boldsymbol{R} = \boldsymbol{R}_{x,\phi}\boldsymbol{R}_{y,\theta}\boldsymbol{R}_{z,\psi}$$

where

$$\boldsymbol{R}_{x,\phi} = \begin{pmatrix} 1 & 0 & 0 \\ 0 & \cos\phi & \sin\phi \\ 0 & -\sin\phi & \cos\phi \end{pmatrix}, \quad \boldsymbol{R}_{y,\theta} = \begin{pmatrix} \cos\theta & 0 & -\sin\theta \\ 0 & 1 & 0 \\ \sin\theta & 0 & \cos\theta \end{pmatrix}, \quad \text{and}$$
$$\boldsymbol{R}_{z,\psi} = \begin{pmatrix} \cos\psi & \sin\psi & 0 \\ -\sin\psi & \cos\psi & 0 \\ 0 & 0 & 1 \end{pmatrix}$$

Letting $\boldsymbol{V} = (U, V, W)^T$ and $\boldsymbol{v} = (u, v, w)^T$ represent inertial velocity expressed in the inertial and body frames, respectively, we have $\boldsymbol{v} = \boldsymbol{R}\boldsymbol{V}$. Letting $\boldsymbol{\omega} = (p, q, r)^T$ represent the body angular velocity, expressed in the body frame, the rates of change of the roll angle ϕ, the pitch angle θ, and the yaw angle ψ are (Etkin 1972):

$$\begin{aligned} \dot{\phi} &= p + q\sin\phi\tan\theta + r\cos\phi\tan\theta \\ \dot{\theta} &= q\cos\phi - r\sin\phi \\ \dot{\psi} &= (q\sin\phi + r\cos\phi)\sec\theta \end{aligned}$$

The dynamic equations for the main body, with the simplified wing dynamic model are

$$\begin{aligned} F_x &= m(\dot{u} + qw - rv) + mg\sin\theta \\ F_y &= m(\dot{v} + ru - pw) - mg\cos\theta\sin\phi \\ F_z &= m(\dot{w} + pv - qu) - mg\cos\theta\cos\phi \\ M_x &= I_x\dot{p} - I_{zx}(\dot{r} + pq) - (I_y - I_z)qr \\ M_y &= I_y\dot{q} - I_{zx}(r^2 - p^2) - (I_z - I_x)rp \\ M_z &= I_z\dot{r} - I_{zx}(\dot{p} - qr) - (I_x - I_y)pq \\ M_{\beta,\mathrm{rw}} &= I^{\mathrm{w}}_{z_\mathrm{b}}\ddot{\beta}_{\mathrm{rw}} \\ M_{\beta,\mathrm{lw}} &= I^{\mathrm{w}}_{z_\mathrm{b}}\ddot{\beta}_{\mathrm{lw}} \end{aligned} \tag{29}$$

where I_x, I_y, and I_z are the mass moments of inertia about the x_b-, y_b-, and z_b-axes, respectively, and I_{zx} is the product of inertia about z–x-axes. The terms F_x, F_y, F_z are the aerodynamic force components and M_x, M_y, M_z are the aerodynamic moment components in the body frame. Finally, $M_{\beta,\mathrm{rw}}$ and $M_{\beta,\mathrm{lw}}$ are the control forces applied on the right and left wings, respectively.

6.2 Control of Three-Dimensional Motion

Motion control in 3-D is carried out by decomposing the motion of the wings into symmetric and asymmetric parts. The symmetric part of the wings' motion is used to control the longitudinal degrees of freedom, as discussed in Sect. 5, while the asymmetric part is used to control roll, yaw, and lateral translation. Suppose the vehicle is to follow a slowly varying yaw angle $\psi_{\mathrm{d}}(t)$. When the wings undergo symmetric motion (as in the case of longitudinal motion), the net aerodynamic moment generated about z_b-axis by the wings is zero. The lateral aerodynamic forces generated along y_b-axis by the two wings are equal and opposite, and therefore cancel each other. If the wings perform slightly asymmetric motions, however, the net aerodynamic moment along z_b-axis and the net lateral force will no longer be zero. The resulting aerodynamic moment and force cause the vehicle to rotate about the z_b-axis (yaw motion) and translate along the y_b-axis (lateral motion). The yaw motion of the vehicle can be controlled by generating a proper aerodynamic moment about the z_b-axis. By using different feather angles η_{rw} and η_{lw} for the two wings, a proper aerodynamic moment can be generated to effect the desired yaw motion. By defining the asymmetric part of the wings' feather angles as

$$\eta_\psi = k_{p_\psi}(\psi_{\mathrm{d}} - \psi) + k_{d_\psi}(\dot{\psi}_{\mathrm{d}} - \dot{\psi})$$

where k_{p_ψ} and k_{d_ψ} are control parameters to be determined, the wings' feather angles can be considered as

$$\begin{aligned}\eta_{\mathrm{rw}} &= \eta_s + \eta_x + \eta_\psi\\ \eta_{\mathrm{lw}} &= \eta_s + \eta_x - \eta_\psi\end{aligned}$$

The slight difference in the wings' feather angles caused by η_ψ generates an aerodynamic moment about z_b-axis to follow the desired yaw angle ψ_{d}. But it also causes a roll motion which generates a lateral force in its turn, causing the vehicle to deviate from its desired trajectory along y_b-axis. The control of the lateral motion of the vehicle can be done by changing the roll angle of the body. A nonzero roll angle of the vehicle causes a nonzero component of the aerodynamic force along the y_b-axis (lateral force). By control of the roll angle, one can control this lateral force to generate (or arrest) lateral motion of the vehicle. To this end, the desired roll angle ϕ_{d} at each time is defined as

$$\phi_{\mathrm{d}} = k_{p_y}(y_{\mathrm{d}} - y) + k_{d_y}(\dot{y}_{\mathrm{d}} - \dot{y}) \tag{30}$$

where k_{p_y} and k_{d_y} are control parameters and y_{d} is the y component of the desired position vector in the rotating $\{x, y, z\}$ frame. By considering $\boldsymbol{X}_{\mathrm{d}} = (X_{\mathrm{d}}, Y_{\mathrm{d}}, Z_{\mathrm{d}})^T$ as the desired position vector in the inertial frame, the desired "quasi-position" vector in the rotating frame $\{x, y, z\}$ is

$$\boldsymbol{x}_{\mathrm{d}} = (x_{\mathrm{d}}, y_{\mathrm{d}}, z_{\mathrm{d}})^T = \boldsymbol{R}^T \boldsymbol{X}_{\mathrm{d}}$$

In this paper, the control of the roll angle is performed by using different amplitudes for the wings' stroke angles β_{rw} and β_{lw}. Different stroke amplitudes generate different aerodynamic forces at the right and left sides of the body, which cause the rotation of the body about the x_b-axis (roll motion). Using the desired roll angle ϕ_{d} defined by (30), the asymmetric part of the stroke angle is defined as

$$\beta_\phi = k_\phi(\phi_{\mathrm{d}} - \phi)$$

where k_ϕ is a constant parameter. Using β_ϕ, the control moments applied to the wings are determined as

$$\begin{aligned} M_{\beta,\mathrm{rw}}(t) &= k_{p_{\beta,r}}\beta_{\mathrm{rw}} + k_{d_{\beta,r}}\dot{\beta}_{\mathrm{rw}} + B_0(t)\left(1 + k_{p_z}\left(Z_{\mathrm{d}}(t) - Z\right)\right. \\ &\quad \left. + k_{d_z}\left(\dot{Z}_{\mathrm{d}}(t) - \dot{Z}\right) - \beta_\phi\right)\omega\cos\omega t \\ M_{\beta,\mathrm{lw}}(t) &= k_{p_{\beta,l}}\beta_{\mathrm{lw}} + k_{d_{\beta,l}}\dot{\beta}_{\mathrm{lw}} + B_0(t)\left(1 + k_{p_z}\left(Z_{\mathrm{d}}(t) - Z\right)\right. \\ &\quad \left. + k_{d_z}\left(\dot{Z}_{\mathrm{d}}(t) - \dot{Z}\right) + \beta_\phi\right)\omega\cos\omega t \end{aligned}$$

Substituting these control moments into equations of motion (29), one can transform these equations to the standard averaging form of (24) with the averaged approximation of (25). Then one may seek control parameter values that enable the system to meet stability and performance requirements.

6.3 Numerical Results for the Three-Dimensional Motion

Using the control method described for 3-D motion, the vehicle can turn in hover or during forward motion. In this section, the results of following two such trajectories are presented. The physical parameters are

$$\begin{gathered} I_x = 1.5\times10^{-6}\,\mathrm{kg\,m^2}, \quad I_z = 1.2\times10^{-6}\,\mathrm{kg\,m^2}, \quad I_{zx} = -0.02I_x \\ k_{p_\psi} = 1, \quad k_{d_\psi} = 1, \quad k_{p_y} = 0.6, \quad k_{d_y} = 0.4 \quad k_\phi = 20 \end{gathered}$$

The rest of the physical parameters are the same as in Sect. 5.2. For the simulations, as before, the body's motion was incorporated when computing the wing angle of attack:

$$\begin{aligned} \eta_{\mathrm{rw}} &= \eta_s + \alpha_{\mathrm{b_{rw}}} + \eta_x + \eta_\psi \\ \eta_{\mathrm{lw}} &= \eta_s + \alpha_{\mathrm{b_{lw}}} + \eta_x - \eta_\psi \end{aligned}$$

where $\alpha_{\mathrm{b_{rw}}}$ and $\alpha_{\mathrm{b_{lw}}}$ are the contributions to wing angle of attack due to the base body translation and rotation.

In the first simulation, the desired trajectory is a concatenation of straight and harmonic ascending and descending flight segments, interspersed with turning maneuvers in hovering flight. The simulation results in Figs. 5 and 6 exhibit effective trajectory following.

For the second simulation, the desired trajectory begins with straight forward motion and continues into an ascending helical trajectory. The required yaw angle during the

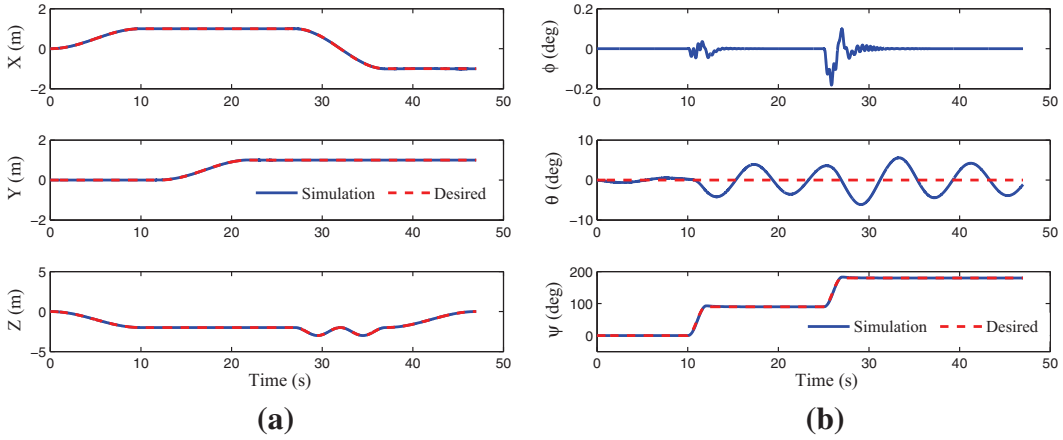

Fig. 5 Simulation results for trajectory 1. Time histories of **a** X, Y, and Z, **b** ϕ, θ, and ψ

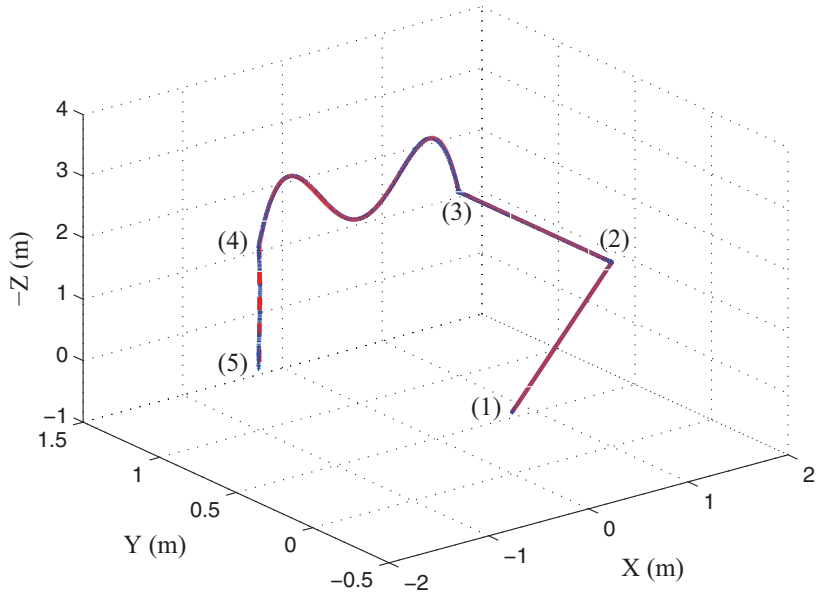

Fig. 6 3-D trajectory 1 of the BAV (*full-blue*: simulation, *dashed-red*: desired) (Color figure online)

helical motion is $\psi_{\mathrm{d}}(t) = \tan^{-1}\frac{v_{\mathrm{d}}(t)}{u_{\mathrm{d}}(t)}$, where u_{d} and v_{d} are the body frame components of the desired translational velocity. Again, Figs. 7 and 8 illustrate effective trajectory following.

7 Conclusion

An approach to three-dimensional flight control for a biomimetic air vehicle was developed by treating the vehicle as a vibrational control system—a mechanical system subject to high-frequency, high-amplitude forcing. First, the longitudinal equations of motion were developed and then simplified by omitting the inertial effects of the wings. Using this simplified model, a trajectory tracking controller was developed using two of the wings' three degrees of freedom: wing stroke (or flapping) motion and wing feather (or pitch) motion. Modulating the amplitude of the stroke angle enables

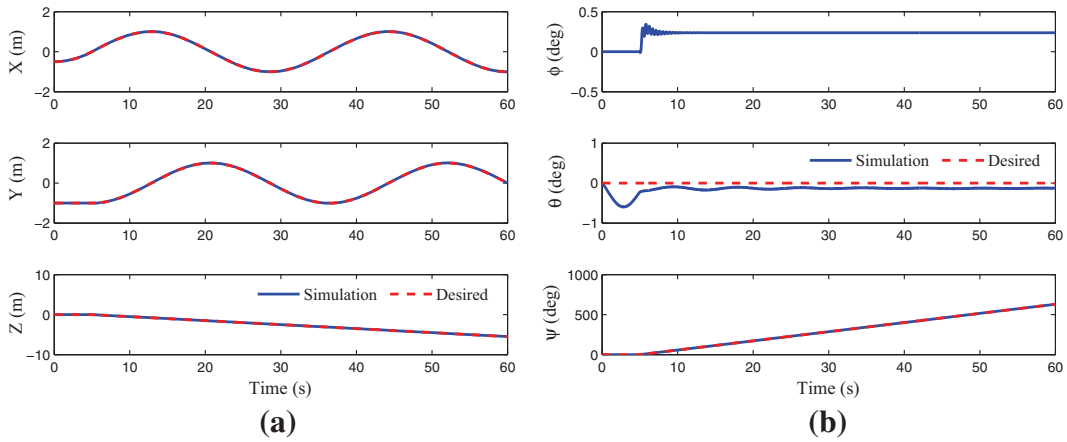

Fig. 7 Simulation results for trajectory 2. Time histories of **a** X, Y, and Z, **b** ϕ, θ, and ψ

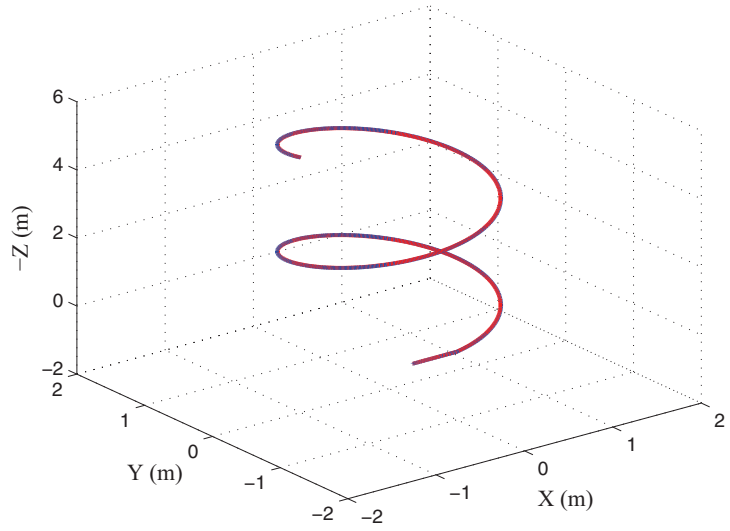

Fig. 8 3-D trajectory 2 of the BAV (*full-blue*: simulation, *dashed-red*: desired) (Color figure online)

control of vertical motion, while the amplitude of the feather angle allows control of horizontal (forward) motion. The control method was implemented in simulation using equations that include multi-body effects. Results suggest that the proposed controller is robust to model uncertainty. The controller developed for longitudinal flight was then extended to enable three-dimensional trajectory tracking. In this case, differential motion of the wings was incorporated to enable control of yaw, roll, and lateral translation. In simulations, the controller enabled turning flight in hover and in forward, climbing flight. As future work, one may consider more realistic kinematics for the wing feathering (pitch) motion. Using fewer actuators, thereby decreasing the vehicle weight, is also a significant goal for future work.

Acknowledgements The authors gratefully acknowledge the comments of the anonymous reviewers and the support of the National Science Foundation under Grant No. CMMI-1435484. The authors also would like to thank Dr. Haithem Taha for helpful discussions.

References

Anderson, M.L., Cobb, R.G.: Toward flapping wing control of micro air vehicles. J. Guid. Control Dyn. **35**(1), 296–308 (2012)

Anderson, M.L., Cobb, R.G.: Implementation of a flapping wing micro air vehicle control technique. J. Guid. Control Dyn. **37**(1), 290–300 (2014)

Berman, G.J., Wang, Z.J.: Energy-minimizing kinematics in hovering insect flight. J. Fluid Mech. **582**, 153–168 (2007)

Bhatia, M., Patil, M., Woolsey, C., Stanford, B., Beran, P.: Stabilization of flapping-wing micro-air vehicles in gust environments. J. Guid. Control Dyn. **37**(2), 592–607 (2014)

Bullo, F.: Averaging and vibrational control of mechanical systems. SIAM J. Control Optim. **41**(2), 542–562 (2002)

Bullo, F., Lewis, A.D.: Geometric Control of Mechanical Systems. Texts in Applied Mathematics, vol. 49, pp. 467–471. Springer, New York, NY (2005)

Chirarattananon, P., Ma, K.Y., Wood, R.J.: Adaptive control of a millimeter-scale flapping-wing robot. Bioinspir. Biomimet. **9**(2), 025004 (2014)

Deng, X., Schenato, L., Sastry, S.S.: Flapping flight for biomimetic robotic insects, part 2: flight control design. IEEE Trans. Robot. **22**(4), 789–803 (2006a)

Deng, X., Schenato, L., Wu, W.C., Sastry, S.S.: Flapping flight for biomimetic robotic insects, part 1: system modeling. IEEE Trans. Robot. **22**(4), 776–788 (2006b)

Dickinson, M.H., Lehmann, F.O., Sane, S.P.: Wing rotation and the aerodynamic basis of insect flight. Science **284**(5422), 1954–1960 (1999)

Doman, D.B., Oppenheimer, M.W., Sigthorsson, D.O.: Wingbeat shape modulation for flapping-wing micro-air-vehicle control during hover. J. Guid. Control Dyn. **33**(3), 724–739 (2010)

Ellington, C.P.: The aerodynamics of the hovering insect flight. I. the quasi-steady analysis. Philos. Trans. R. Soc. B Biol. Sci. **305**(1122), 1–15 (1984)

Elzinga, M.J., van Breugel, F., Dickinson, M.H.: Strategies for the stabilization of longitudinal forward flapping flight revealed using a dynamically-scaled robotic fly. Bioinspir. Biomimet. **9**(2), 025001 2014

Etkin, B.: Dynamics of Atmospheric Flight. Wiley, New York (1972)

Greenwood, D.T.: Advanced Dynamics. Cambridge University Press, Cambridge, UK (2003)

Guckenheimer, J., Holmes, P.: Nonlinear Oscillations, Dynamical Systems, and Bifurcations of Vector Fields. Applied Mathematical Sciences, vol. 42, pp. 166–169. Springer, New York, NY (1983)

Jenkins, C.: Bio-inspired Engineering. Momentum Press, New York (2011)

Keennon, M., Klingebiel, K., Won, H., Andriukov, A.: Development of the nano hummingbird: a tailless flapping wing micro air vehicle. In: Proceedings of AIAA Aerospace Science Meeting, Nashville, TN. AIAA 2012-0588, January 2012

Khan, Z.A., Agrawal, S.K.: Control of longitudinal flight dynamics of a flapping-wing micro air vehicle using time-averaged model and differential flatness based controller. In: Proceedings of American Control Conference, pages 5284–5289, New York City, NY, July 2007

Ma, K.Y., Chirarattananon, P., Fuller, S.B., Wood, R.J.: Controlled flight of a biologically inspired insect-scale robot. Science **340**, 603–607 (2013)

Oppenheimer, M.W., Doman, D.B., Sigthorsson, D.O.: Dynamics and control of a minimally actuated biomimetic vehicle: Part II—control. In: Proceedings of AIAA Guidance, Navigation, and Control Conference, Chicago, IL. AIAA 2009-6161, August 2009

Oppenheimer, M.W., Doman, D.B., Sigthorsson, D.O.: Dynamics and control of a biomimetic vehicle using biased wingbeat forcing functions. J. Guid. Control Dyn. **34**(1), 204–217 (2011)

Orlowski, C.T., Girard, A.R.: Dynamics, stability, and control analyses of flapping wing micro-air vehicles. Prog. Aerosp. Sci. **51**, 18–30 (2012)

Ramamurti, R., Sandberg, W.C.: A three-dimensional computational study of the aerodynamic mechanisms of insect flight. J. Exp. Biol. **205**(10), 1507–1518 (2002)

Rifai, H., Marchand, N., Poulin-Vittrant, G.: Bounded control of an underactuated biomimetic aerial vehicle—validation with robustness tests. Robot. Auton. Syst. **60**(9), 1165–1178 (2012)

Sanders, J.A., Verhulst, F.: Averaging Methods in Nonlinear Dynamical Systems. Applied Mathematical Sciences, vol. 59, pp. 33–66. Springer, New York, NY (1985)

Serrani, A., Keller, B.E., Bolender, M.A., Doman, D.B. : Robust control of a 3-dof flapping wing micro air vehicle. In: Proceedings of AIAA Guidance, Navigation, and Control Conference, Toronto, Canada. AIAA 2010-7709, August 2010

Sun, M.: Insect flight dynamics: stability and control. Rev. Mod. Phys. **86**, 615–646 (2014)

Sun, M., Wang, J., Xiong, Y.: Dynamic flight stability of hovering insects. Acta Mech. Sin. **23**(3), 231–246 (2007)

Taha, H.E., Hajj, M.R., Nayfeh, A.H.: Flight dynamics and control of flapping-wing MAVs: a review. Nonlinear Dyn. **70**(2), 907–939 (2012)

Tahmasian, S., Woolsey, C.A.: A control design method for underactuated mechanical systems using high frequency inputs. ASME J. Dyn. Syst. Meas. Control **137** (2015). doi:10.1115/1.4029627

Tahmasian, S., Taha, H.E., Woolsey, C.A.: Control of underactuated mechanical systems using high frequency input. In: Proceedings of IEEE American Control Conference, pp. 603–608, Washington, DC, June 2013

Tahmasian, S., Allen, D.W., Woolsey, C.A.: On averaging and input optimization of high-frequency mechanical control systems. J. Vib. Control (2016). doi:10.1177/1077546316655706

Ward, T.A., Rezadad, M., Fearday, C.J., Viyapuri, R.: A review of biomimetic air vehicle research: 1984–2014. Int. J. Micro Air Veh. **7**(3), 375–394 (2015)

Wood, R.J.: The first takeoff of a biologically inspired at-scale robotic insect. IEEE Trans. Robot. **24**(2), 341–347 (2008)